JOURNAL OF CATALYSIS 140, 543–556 (1993)

Catalyzed Carbon Gasification Studied by Scanning Tunneling Microscopy and Atomic Force Microscopy

X. CHU,* L. D. SCHMIDT,*,[1] S. G. CHEN,† AND R. T. YANG†,[1]

*Department of Chemical Engineering and Materials Science, University of Minnesota, Minneapolis, Minnesota 55455; and †Department of Chemical Engineering, State University of New York at Buffalo, Buffalo, New York 14260

Received July 13, 1992; revised November 20, 1992

Several important catalyzed gas–carbon reactions are studied by scanning tunneling microscopy (STM) and atomic force microscopy (AFM): $C/H_2/Pt$, $C/H_2/Pd$, $C/O_2/V_2O_5$, $C/CO_2/K_2CO_3$, and C/NO/Rh. Single-crystal graphite is used as a prototype of carbon in the reactions. STM and AFM provide atomic resolution in three dimensions, making possible the direct identification of monolayer and multilayer structures on the reacted graphite surface. Reactions take place on the basal plane of graphite through monolayer and multilayer channeling, pitting, and edge recession. Therefore, by examining the etched surface structures of graphite after different reactions, reaction pathways and reaction parameters can be determined. It has been found that channeling is the primary contribution to the gasification rate in all these reactions. Two different modes of channeling are found. For reactions in $C/H_2/Pt$, $C/H_2/Pd$, $C/O_2/V_2O_5$ systems, catalyst particles remain unchanged in size. Thus, the resulting channels either have constant-width or form zig-zag structures due to the changes of the motion of catalyst particles. However, for reactions in the $C/CO_2/K_2CO_3$ and C/NO/Rh systems, wedge-shaped channels are produced. This indicates that the catalyst particles are shrinking in size, either because of volatilization or deposition of catalyst at the step edge.

1. INTRODUCTION

Carbon gasification is greatly enhanced by the presence of catalysts (*1–3*), and much attention has focused on the effects of metals, metal oxides, and salts in gas–carbon reactions. The most important gas–carbon reactions are associated with energy production involving O_2, CO_2, H_2O, or H_2 as reactants, and also pollution elimination involving NO_x and SO_2. Much of our present understanding of the catalytic behavior is obtained from microscopy. These studies have progressed from optical microscopy (*4*) to various techniques of electron microscopy, e.g., gold-decoration TEM (*5*) and controlled-atmosphere TEM (*6*).

A unique and intriguing phenomenon associated with catalyzed gas–graphite reactions is the motion of the catalyst particles on the graphite which produces catalytic activity. The most extensively studied catalyst actions are pitting (*1*, *7*), deep channeling (*8*, *9–12*), and deep edge recession (*13*, *14*). The two latter refer to the carving of channels and receding of line edges by the catalysts, both of which involve many graphite layers, hence the term "deep." These processes have been studied mainly by controlled-atmosphere TEM.

Controlled-atmosphere TEM relies on the relative thickness contrast of images which requires channels many graphite layers deep (typically > 30 layers) and consequently overlooks catalytic events occuring on the surface layers of graphite. By using gold decoration, monolayer (single graphite layer) processes, including channeling, edge recession, and pitting, have been revealed, and the kinetics and mechanism of monolayer channeling in a number of important reactions have been reasonably well charac-

[1] To whom correspondence should be addressed.

0021-9517/93 $5.00

terized (*15–19*). The contribution to the overall gasification rates by monolayer channeling has also been found to be important. While deep channeling is initiated by catalyst particles located at multilayer steps on the basal plane of graphite, monolayer channeling is initiated from both lattice vacancies and monolayer steps (*16*). The unbalanced adhesion force acting upon the particle (only the front portion of the particle is in contact with the edge atoms of graphite) is the driving force for its motion (*16*). For all the reactions that have been investigated, the total carbon gasification rates are equal for the same-sized particles undergoing channeling at different depths (*16–19*); hence monolayer channeling is more rapid than deep channeling.

All of the microscopic techniques described above provide only a two-dimensional view. Scanning tunneling microscopy (STM) can provide additional information on the vertical dimension. STM has been employed to study graphite supported metal particles and the catalytically etched deep channel structures (*20*, *21*) as well as the step structures of oxidized graphite surface (*22*). STM has also been used to provide direct proof that uncatalyzed etched pits on the basal plane are one monolayer deep (*23*, *24*). More recently, STM has also been used to study the kinetics of both uncatalyzed and catalyzed gas–graphite reactions (*24*, *25*). For catalyzed reactions, primarily deep channels have been observed on a pyrolytic graphite.

In this work, STM and atomic force microscopy (AFM) studies are performed on single crystals of graphite for several important catalyzed gas–carbon reactions. It will be demonstrated that both STM and AFM are capable of yielding unique information on the gasification of graphite for several catalyst materials.

2. EXPERIMENTAL

For the reactions in the Pt-graphite/H_2, V_2O_5–graphite/O_2 and K_2CO_3–graphite/CO_2 systems natural single-crystal graphite from Ticonderoga, New York, was used. The sample pretreatment procedure was as described previously (*27*) except repeated cleavages were not required for STM because single cleavages provided large and smooth basal plane surfaces. The same systems have been studied in detail by using the gold-decoration TEM technique (*16–19*).

The Pt was 99.99% purity while V_2O_5, K_2CO_3 were both of puratronic grade with purities 99.9%. The detailed procedures for catalysts deposition on the graphite basal plane upon H_2 treatment at 900°C has been described previously (*16*). The V_2O_5 catalyst was deposited using a suspension of V_2O_5 powder in alcohol, and the K_2CO_3 was deposited from aqueous solution. Subsequent heat treatments were employed to ensure catalyst dispersion (*18*, *19*).

The prepared samples were placed on a sapphire plate and initially degassed in He at 500°C for 12 hr. Reactions were carried out in a tube furnace with He carrier gas of O_2-free grade with a minimum purity of 99.995% and a maximum O_2 content of 0.5 ppm. The H_2 was of ultrahigh purity (99.999%), and the CO_2 and O_2 had a minimum purity of 99.99%.

For reactions in the C/H_2/Pd and C/NO/Rh systems, highly orientated pyrolytic graphite obtained from Union Carbide (grade ZYA) was used. High purity Pd (99.95%) and Rh (99.95%) were vacuum-deposited on freshly cleaved samples. The samples were then heated in high purity He (99.999%) at 300 to 350°C for 2 to 10 hr to convert the deposited thin metal films into small particles. The samples with Pd were then heated in pure H_2 at 400°C for 30 hr. The samples with Rh were heated in a mixture of 5% NO in He at atmospheric pressure at specified temperatures and times. Since the presence of O_2 enhances the etching rate, high purity He gas was used first for at least 30 min to flush out the residual air and heat the sample to the reaction temperature. The reacting gases were admitted when the system achieved the reaction tem-

perature. After reaction, the reacting gases were removed and the samples were quenched in He to room temperature. These procedures assured that there was no significant reaction caused by gaseous impurities in both the annealing and heating processes as examined by STM.

After reaction, the samples were transferred to a Nanoscope II scanning tunneling microscope (STM) which could be operated in STM and AFM modes. All examinations were made in air at 300 K. For STM the constant height mode was used. The scan rate was adjusted for best images as described previously (*24*, *25*).

AFM, unlike STM, can image electric insulators. A sample was scanned with a SiC cantilever. The cantilever tip (which may end in a single atom) presses against individual atoms in the sample, generating a repulsive force that varies with surface relief. The force deflects the tip whose movements are monitored by a laser beam which is reflected from the top of the arm to a path by activating a piezoelectric control which adjusts the sample height so that the deflection of the arm remains constant. The sample movements are translated into a surface profile.

The surfaces were first imaged over about 20 different 15 × 15 μm^2 regions for each sample. Those regions showing interesting structures were then scanned with lower Z ranges and slower scanning rates. Repeated calibrations were made for the step height of graphite. An exponential output of the image was chosen so that monolayer steps could be easily distinguished from double or multilayer structures.

3. RESULTS AND DISCUSSION

The most active catalysts for the gasification of carbon with H_2, O_2, and CO_2 are, respectively, Group VIII metals (for C–H_2 reaction), transition metal oxides (for C–O_2 reaction), and salts of alkali metals (for C–CO_2 reaction). For this reason, the catalysts chosen for this study were, Pt and Pd(C–H_2), V_2O_5(C–O_2), and K_2CO_3(C–CO_2). Also, Rh was studied for the C–NO reaction. Moreover, since these systems have been studied in detail using gold decoration TEM (*15–19*), direct comparisons can be made between the two techniques. Because the C–CO_2 reaction and the C–H_2O reaction are similar for both uncatalyzed and catalyzed reactions, only the C–CO_2 reaction was studied.

Pt-Catalyzed Graphite–H_2 Reaction

A low magnification STM view of a single crystal graphite sample after reaction at 1 atm H_2 at 900°C for 40 min is shown in Fig. 1a along with the STM height profile. The large number of channels resulted from a high concentration of Pt particles deposited on the sample. The channels had a uniform height of 3.4 ± 0.2 Å, indicating that these channels are only one graphite layer (3.35 Å) deep.

The monolayer channels shown in Fig. 1a had specific orientations which propagated along both zigzag and armchair edge plane directions of the graphite. The widths as well as the depths of channels catalyzed by Pt were maintained during channel propagation. This kind of channel is usually created by large catalyst particles. These characteristics were the same as observed using TEM (*16*).

Very few Pt particles (bright dots) were found on the sample because the STM tip caused them to move elsewhere. More particles remained at the ends of multilayer channels (*24*). This may be attributed to the fact that in multilayer channels the particle is bonded to the edges of many layers so that adhesion forces are enhanced.

In addition to the straight constant-width monolayer channels, some irregular monolayer channels were also observed. Figure 1b shows an AFM micrograph of a region in the same sample as shown in Fig. 1a. This kind of channel was produced by many small Pt particles which could still be seen at the edges of the channel walls.

In general, STM gives better images of graphite surfaces with a small height difference such as monolayer steps. However,

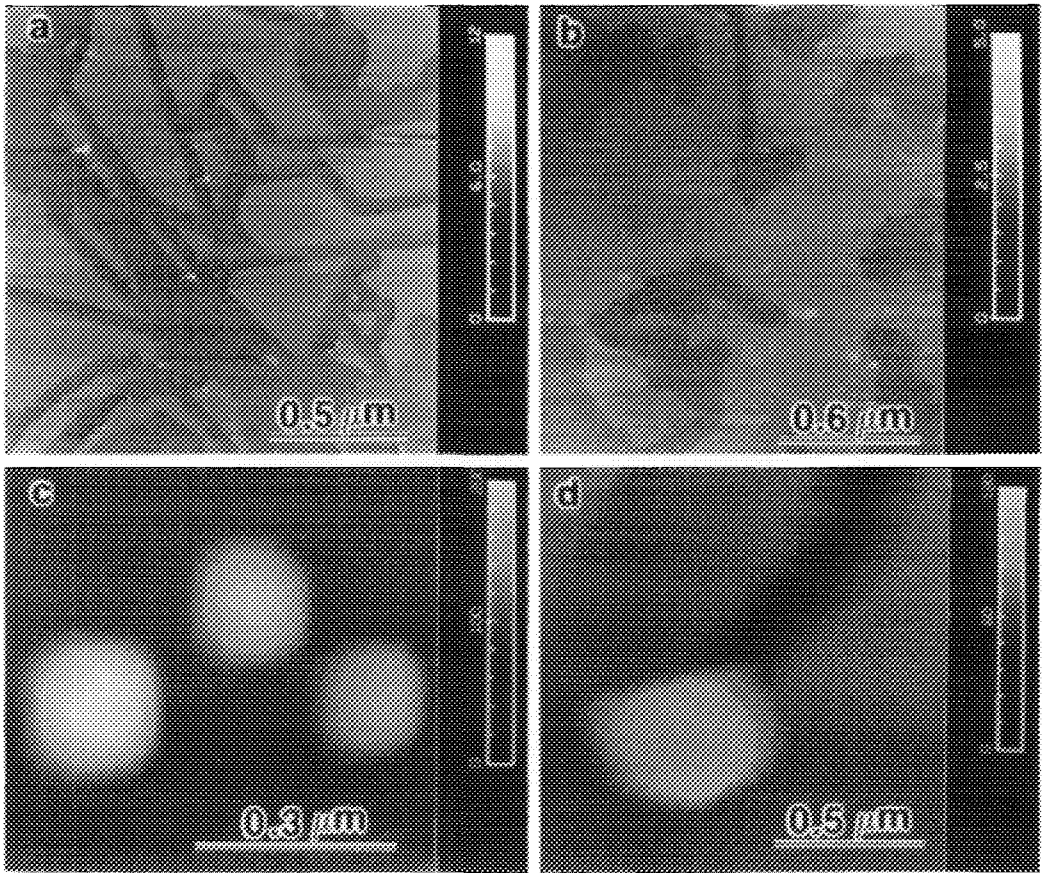

FIG. 1. (a) STM image of straight monolayer channels from a graphite basal plane carved by Pt particles in 1 atm H_2 at 900°C for 40 min with height scale (in nanometers) showing that the channels are one atomic layer deep (3.35 Å). (b) AFM image of irregular monolayer channels in the same sample as (a). (c) AFM image of cube shaped Pt particles on the same sample in (a) and (b). (d) STM image of a multilayer channel on a graphite (ZYA) basal plane etched by a Pt particle (which is at the channel end) in 1 atm H_2 at 850°C for 45 min.

AFM gives good images of large surface height variations such as those over catalyst particles. Figure 1c shows a region on the same sample as in Figs. 1a and 1b where cubic Pt particles are distributed. A three dimensional profile is shown for each particle.

Although multilayer channels were also found on the natural graphite sample, there were more monolayer channels than multilayer channels. However, on highly oriented pyrolytic graphite, mostly multilayer channels were observed. This graphite consisted of small single crystals joined together at an average "mosaic spread (angle)" of 1 degree, i.e., the average angle of alignment at boundaries was 1 degree. These boundaries were formed by joining multilayer edges of two single crystals. Multilayer channels could be initiated from these boundaries. Alternatively, when a monolayer channeling particle crossed a boundary, the ensuing channel was likely to be multilayer. Figure 1d shows a STM image of a multilayer channel produced by a Pt particle. Note that the height scales in Fig.

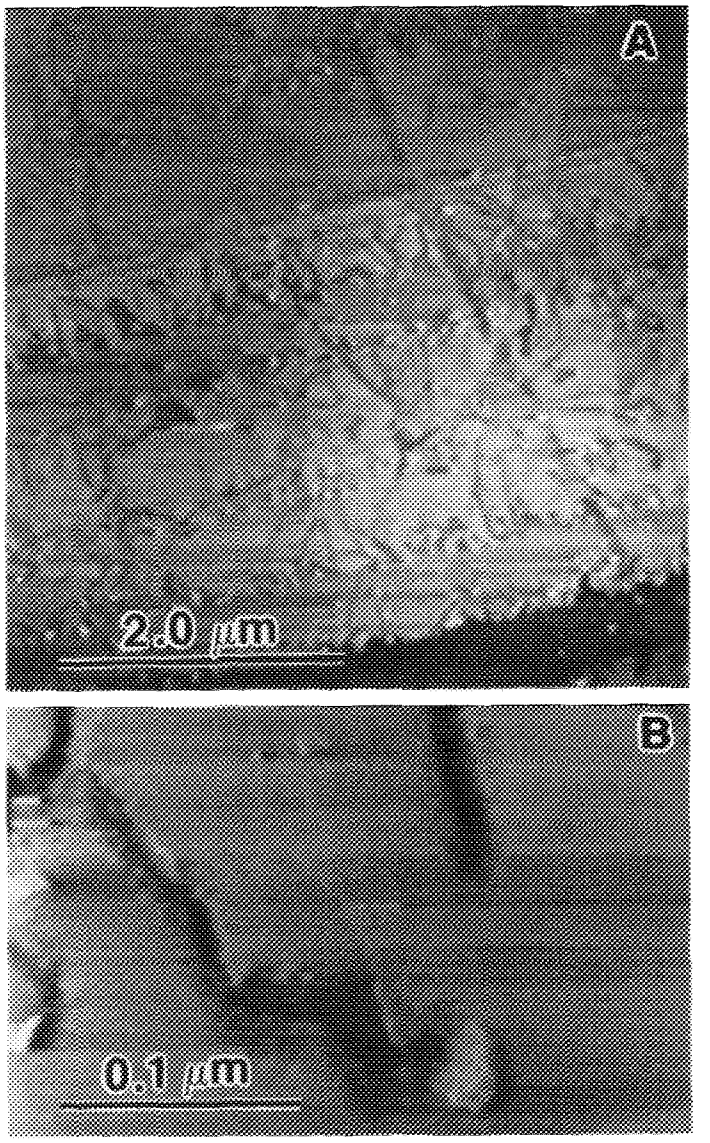

FIG. 2. (a) Low magnification view of a graphite basal plane carved by Pd particles in 1 atm H_2 at 400°C for 30 hr. (b) Enlarged image of a catalyst particle and its created channel.

l are different for the four cases. The wedge-shaped cross section of the channel is visible and the catalyst particle stopped at the end of the channel.

Pd-Catalyzed Graphite–H_2 Reaction

Figure 2a shows a low magnification view of a sample after heating in H_2 at 400°C for 30 hr. Several monolayer steps are shown and monolayer channeling initiated from these monolayer steps. Unlike the uniform, constant-width monolayer channels formed in the Pt catalyzed reactions, the monolayer channels observed here were mostly randomly orientated. They also intersected each other. There were more channels in the

upper atomic layer than the lower atomic layer as indicated by the difference in channel density on each side of the monolayer step.

Figure 2b shows an enlarged region on the same sample shown in Fig. 2a. Several multilayer channels are shown. The large channel with a catalyst particle at its end has a thin and narrow leading edge, indicating the existence of a terraced edge at the metal–graphite interface. Also the channel width and depth altered during propagation, caused by the change of orientations of the catalyst particle.

The dependence of the channeling rate on particle size and channel depth can provide insight into the mechanistic steps and the rate-limiting step involved in the channeling action (*16–19*). For the $Pt/C/H_2$ system, the channeling rate was found to be proportional to particle size (or width), and approximately proportional to the inverse of the depth (*16*).

Unlike TEM, STM provides information on the distribution of channels with different depths. This information is useful in assessing the relative contributions of channeling in different depths toward the overall rates. Determining the channeling rate requires the measurement of channels with clearly defined beginnings and ends. The dense population of the channels on the sample, however, made such measurements difficult. Further quantitative study on the catalytic reactions, especially those at low temperatures and low pressures, is ongoing.

V_2O_5-Catalyzed Graphite–O_2 Reaction

Reaction was carried out in 1 atm air at 500°C for 40 min. Both monolayer and multilayer channels were observed on the samples and they were of approximately equal numbers. Figures 3a and 3b show a step region on the graphite surface where the left-hand side was lower than the right-hand side by two atomic layers (6.7 Å). The rod-shaped catalyst particles observed in TEM studies (*18, 28*) are also seen in Fig. 3. Here all channels initiated from the step. Larger particles channeled at higher rates, resulting in longer channels. Also, monolayer channeling was faster than double layer channeling for the same size catalyst particles. Further, the channeling rate depended on the orientation of the catalyst particles.

Figure 4 shows a region where monolayer and multilayer channels coexisted. Catalyzed edge recessions are also shown in Fig. 4, which exhibits a stepped ledge containing a monolayer edge and a two-layer edge. The traces in the upper right corner (thin white lines) are monolayer ledges resulting from monolayer channeling by many catalyst particles moving in the same direction. The catalyzed edge recession has also been studied using TEM for both monolayer recession (17) and multilayer edge recession (28).

K_2CO_3-Catalyzed Graphite–CO_2 Reaction

This reaction was carried out in 1 atm of CO_2 at 700°C for 40 min. The phenomena involved in the catalyzed $C–H_2O$ reaction are very similar to that of the catalyzed $C–CO_2$ reaction (*19*), so it was not included in this study.

A feature unique to the graphite–CO_2–alkali reaction system is the formation of channels of wedge shape. Wedge-shaped monolayer (*19*) and multilayer (*29*) channels were observed by TEM. The wedged shape indicates that the channel walls also underwent catalyzed recession. Since the channeling walls were covered by the C–O–K phenolate-type groups under the reaction conditions (see Ref. (*19*) for the literature on the identification of these groups), it is concluded that the C–O–K group has a small activity and that particles and clusters (located at the tips of the channels) have high activities (*19*).

STM pictures showed both wedge shaped monolayer channels and wedge shaped multilayer channels. Figure 5 shows a 10 × 10 μm region where wedge shaped channels deeper than five layers were present. Figure 6a is a higher magnification scan of the upper right region of Fig. 5, while Fig. 6b shows a

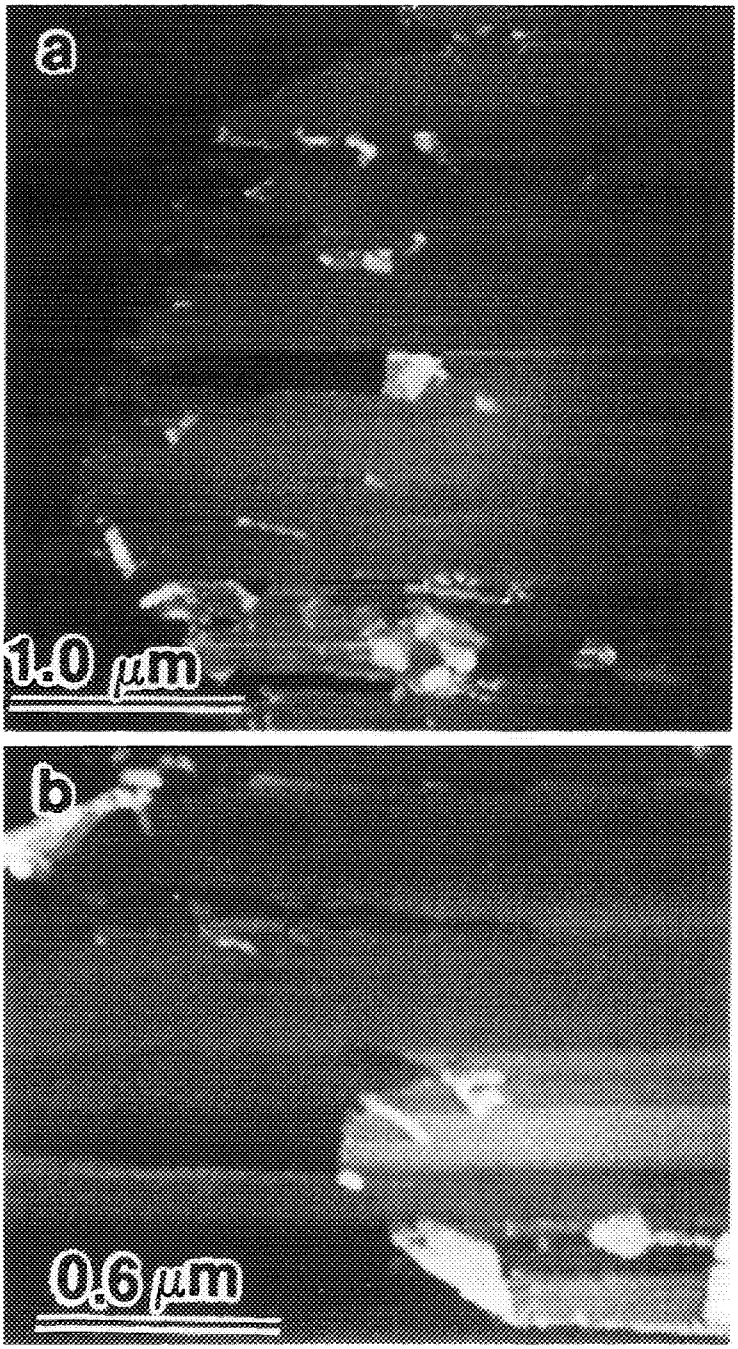

FIG. 3. STM images of channels on graphite basal plane carved by V_2O_5 in 1 atm O_2 at 500°C for 40 min. The ledge on the right consists of two graphite layers, which is the depth of all channels in this region.

FIG. 4. Monolayer and multilayer channels observed in the same sample as shown in Fig. 3. The thin parallel white lines are monolayer ledges created by produced by the motions of V_2O_5 particles moving at the same direction during the catalytic reaction.

region where monolayer and double-layer channels were present. This picture also shows a monolayer channel cutting through a ledge one atomic layer high. In Fig. 6a it is seen that the channel length did not depend on the channel depth. This is consistent with previous TEM results showing that the C–C bond breakage (at the graphite edge-catalyst interface) was the rate-limiting step in alkali catalyzed channeling (*19*).

In addition to monolayer and multilayer channels, monolayer etch pits of elongated hexagonal shape were also observed by STM, as shown in Fig. 7a. A second layer (also of monolayer depth) with an inverted orientation was also observed. These two pits were concentric. This is a common phenomena in many catalyzed gas-graphite reactions (*17*, *18*). The cause of formation of these pits was that two adjacent zigzag edges in the hexagonal pit were different due to different alignments with the underlying graphite lattice (*17*, *18*). A TEM picture of gold decorated pits formed by V_2O_5 with 0.1 atm O_2 at 600°C is shown in Fig. 7b for comparison.

The double-layer pits shown in Fig. 7a were possibly initiated by catalytic abstraction to form vacancies in two graphite layers. The catalyst particle itself would disperse to coat on the monolayer edges of the pit in first layer. The pit in the second layer grew at a slower rate because it had less or no catalyst. This was the case for the K_2CO_3 catalyzed C–CO_2 reaction. However, in the V_2O_5-catalyzed C–O_2 reaction the first layer pit grew at the same rate as the second layer pit. This difference was possibly by the different dispersion abilities of the two catalyst particles.

FIG. 5. Low magnification STM image of multilayer channels on graphite basal plane by K_2CO_3 in 1 atm CO_2 at 700°C for 40 min.

In the noncatalytic reactions of graphite with various gases (*24*, *25*, *30*), double-layer pits with different centers were formed because the second layer pit was created by the recession of the first layer pit, exposing a vacancy on the second layer basal plane. Thus, the first layer and second layer pits were created at different times and had different sizes and relative orientation.

Rh-Catalyzed Graphite–NO Reaction

NO_x removal from high-temperature combustion sources has attracted increasing attention due to mounting environmental concerns. There are many examples such as heavy oil burners and diesel engines where NO_x and soot are both in the exhaust. It has been recently demonstrated that NO_x has very high reaction rates with graphite (*25*, *30*). Thus it is desirable to explore high performance catalysts to promote these reactions. Details of noncatalytic and catalytic reactions of NO_x with graphite will be published elsewhere (*30*). The reaction of NO with graphite catalyzed by Rh is described here to compare different systems.

Reactions of graphite with NO catalyzed by Rh were found extremely rapid. With a 12 Å thin layer of Rh, significant reaction was found on the graphite surface after heating in 5% NO at 400°C for 30 min. Reactions occurred mainly at steps and the rest of the graphite basal plane remained unattacked. The Rh behaved as metal particles with defined shapes shown by both STM and AFM. Figure 8a shows an AFM picture of the etched surface of graphite by Rh after heating in 5% NO at 400°C for 30 min.

At higher temperatures, multilayer channels propagated from steps, and the reaction spread over the whole graphite basal plane. Figure 8b shows an STM picture of a sample

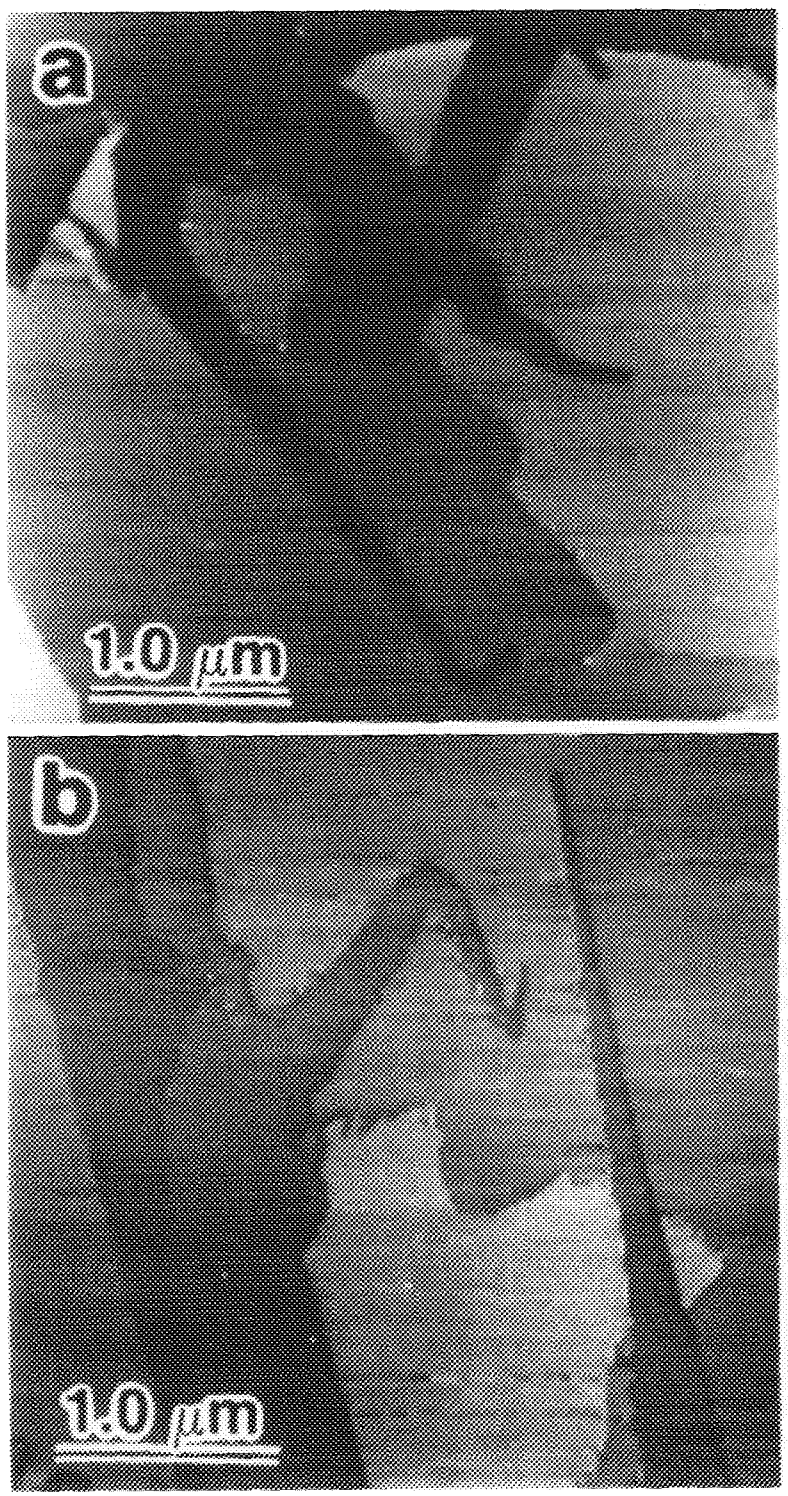

FIG. 6. (a) Enlarged view of a region in Fig. 5, showing multilayer wedge shaped channels produced by K_2CO_3 particles. (b) STM image of another region of the same sample shown in (a), except only monolayer and double-layer channels are shown.

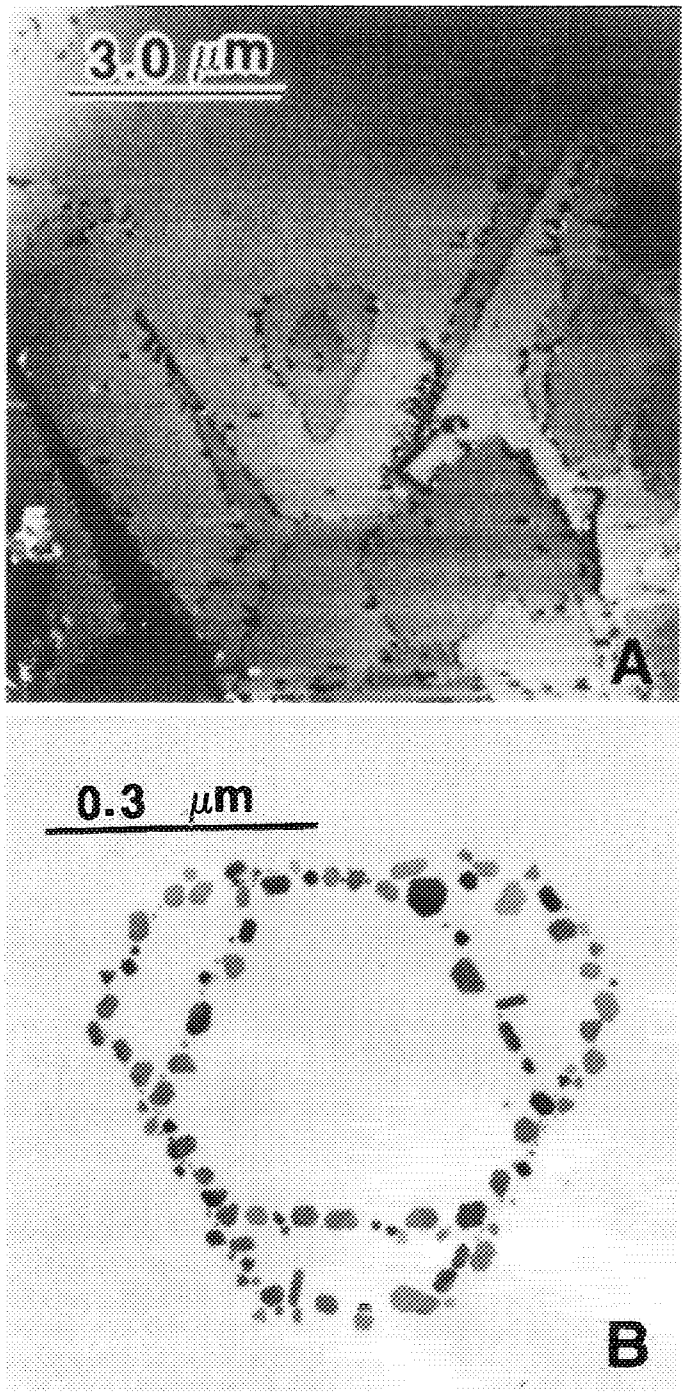

FIG. 7. (a) STM image of another region in the same sample as shown in Fig. 7. Both monolayer and multilayer channels are shown. Also shown is a monolayer elongated hexagonal pit with another monolayer pit inside. (b) TEM picture of gold nuclei decorated on two concentric pits on basal plane from reaction with 0.1 atm O_2 at 600°C catalyzed by V_2O_5.

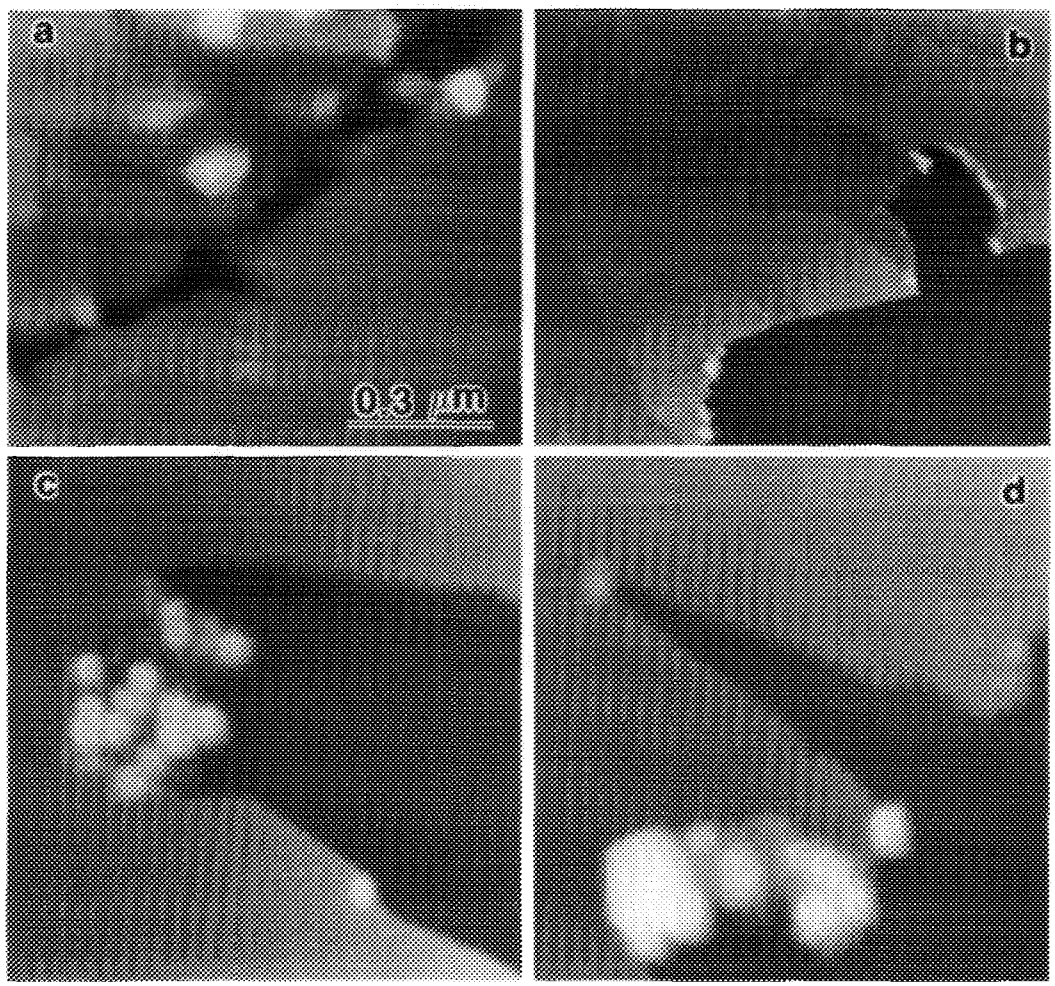

FIG. 8. (a) AFM picture of carved structure of the graphite basal plane by 12-Å film of Rh after reaction in 5% NO at 400°C for 30 min. (b) STM image of the same system after heating in 5% NO at 500°C for 30 min. (c) AFM image of a multilayer channel end on the same sample as shown in Fig. 8b; a cluster of catalytic particles are located at the channel end. (d) A wedge-shaped multilayer channel observed in the same sample as shown in Fig. 8c.

after heating in 5% NO at 500°C for 30 min. Both deep multilayer channels and shallow channels (1 ~ 3 atomic layers) were present. The shallow channels did not propagate in any defined crystallographic orientation as those in the Pt/graphite–H_2 reaction (Fig. 1a). Rather they were similar to those observed previously in the Pt-catalyzed graphite–O_2 reaction (*24*). Shallow channels propagated at higher rates than deep channels, resulting in longer channels.

Two types of multilayer channels were frequently observed on the sample. The first type of multilayer channels have nearly uniform width and were generated by the catalytic reaction of many tiny catalyst particles from a multilayer step. In creating this type of channel all the catalyst particles moved at the same speed. Such an action is illustrated by the AFM picture shown in Fig. 8c. Other types of multilayer channel observed were those with wedge shaped appearance.

One of this type of channel is shown in Fig. 8d. This type of channel was generated by catalyst particles with decreasing size during the catalytic channeling. This kind of channels has been observed in the K_2CO_3 catalyzed C–CO_2 reaction. This is the first observation of this phenomenon in metal catalyzed graphite–NO gasification.

It is interesting to note that the size reduction and even disappearance of Rh particles have been observed in several different systems (31), and two reasons have been suggested for this morphological change during reaction. First, Rh dispersed as atomic species which spread over the support. In this case, Rh possibly wetted the channel walls, as also observed in graphite gasification with H_2 catalyzed by Ni (*32*), with various gases catalyzed by Ba (*29*), and with O_2 catalyzed by Rh (*33*). There are similarities between the Rh/C/NO system and the Rh/C/O_2 system. In the latter, Rh_2O_3 was formed at temperatures below 1000°C (*33*). Second, Rh could react with CO, a reaction product, to form volatile compounds such as carbonyls which would evaporate during the reaction.

4. SUMMARY

Both STM and AFM techniques have been found capable of producing three dimensional atomic structures in catalytic gasification of the basal plane of graphite so that quantitative reaction parameters are readily obtainable. The extreme sensitivities of STM and AFM to surface structures can also be used as a precise means of detecting monolayer catalytic events and evaluating the microstructures with different catalysts involved in reactions with carbon.

In all of the catalytic systems we have studied, catalytic activities involve the motions of the catalyst particles. This has significance in two aspects: first, the catalyst motion itself is a strong reaction parameter and second, the exposed channels act as the new active sites for noncatalytic reactions or for catalytic reaction if the catalyst particles are spread over the exposed surfaces. In addition, large catalyst particles produce higher rates of etching than do small particles. This means high catalyst loading is needed. However, for a fixed catalyst loading, larger catalyst particles reduce the total number of catalytic channels and thus the total exposed atomic active sites are reduced, while if the catalyst particle are too small that they may lose catalytic properties. Therefore, it is crucial to control the distribution of the catalyst particle size in the reaction so that these two aspects can be balanced in order to obtain the best catalytic performances.

ACKNOWLEDGMENTS

This research was supported by NSF under Grants CBT-882745, CTS-9120452, and INT-9000511, and by a grant from Ford Motor Company. We are indebted to T. Tu for help and Dr. Peter J. Goethel (now at Dupont) for Fig. 7b.

REFERENCES

1. Walker, P. L., Jr., Rusinko, F., Jr., and Austin, L. G., *Adv. Catal.* **11,** 133 (1959).
2. Walker, P. L., Jr., Shelef, M., and Anderson, R. A., *in* "Chemistry and Physics of Carbon" (P. L. Walker, Jr., Ed.). Dekker, New York, 1968.
3. Figuereido, J. L., and Moulijn, J. A., "Carbon and Coal Gasification: Science and Technology," NATO ASI Series E, No. 105. Martinus Nighoff, The Netherlands, 1986.
4. Hennig, G. R., *in* "Proc. Conf. Carbon, 1st and 2nd, Buffalo, 1953, 1955," p. 112, 1956.
5. Hennig, G. R., in "Chemistry and Physics of Carbon" (P. L. Walker, Jr., Ed.), Vol. 2. Dekker, New York, 1966.
6. Baker, R. T. K., *Catal. Rev. Sci. Eng.* **19**(2), 161 (1979).
7. Thomas, J. M., in "Chemistry and Physics of Carbon" (P. L. Walker, Jr., Ed.), Vol. 1. Dekker, New York, 1965.
8. Baker, R. T. K., *in* "Carbon and Coal Gasification: Science and Technology," NATO ASI Series E, No. 105. Martinus Nighoff, The Netherlands, 1986.
9. Hennig, G. R., *J. Inorg. Nul. Chem.* **24,** 1129 (1962).
10. McKee, D. W., *in* "Chemistry and Physics of Carbon" (P. L. Walker, Jr., and P. A. Thrower, Ed.), Vol. 16. Dekker, New York, 1980.
11. Keep, C. W., Terry, S., and Wells, M., *J. Catal.* **66,** 451 (1980).
12. Coates, D. J., Evans, J. W., Cabrera, A. L., Somorjai, G. A., and Heinemann, H., *J. Catal.* **80,** 215 (1983).

13. Harris, P. S., Feates, F. S., and Reuben, B. G., *Carbon* **11,** 565 (1973).
14. Baker, R. T. K., *Carbon* **24,** 715 (1986).
15. Yang, R. T., and Wong, C., *J. Catal.* **85,** 154 (1984).
16. Goethel, P. J., and Yang, R. T., *J. Catal.* **101,** 342 (1986).
17. Goethel, P. J., and Yang, R. T., *J. Catal.* **119,** 201 (1989).
18. Pan, Z. J., and Yang, R. T., *J. Catal.* **130,** 161 (1991).
19. Chen, S. G., and Yang, R. T., *J. Catal.*, in press.
20. Bailey, J. M., and Schmidt, L. D., *in* "Proc. 47th Ann. Mtg. Electron Microscopy Soc. Am." San Francisco Press, San Francisco, 1989.
21. Bailey, J. M., M.S. thesis, University of Minnesota, Minneapolis, MN, 1989.
22. Porte, L., Richard, D., and Gallezot, P., *J. Microsc.* **152,** 515 (1988).
23. Chang, H., and Bard, A. J., *J. Am. Chem. Soc.* **112,** 4598 (1990); **113,** 5588 (1991).
24. Chu, X., and Schmidt, L. D., *Carbon* **29,** 1251 (1991).
25. Chu, X., and Schmidt, L. D., *Surf. Sci.* **268,** 325 (1992).
26. Hennig, G. R., *J. Chem. Phys.* **40,** 2877 (1964).
27. Yang, R. T., *in* "Chemistry and Physics of Carbon" (P. L. Walker, Jr., Ed.), Vol. 19, p. 163. Dekker, New York, 1984.
28. Baker, R. T. K., Thomas, R. B., and Wells, M., *Carbon* **13,** 141 (1975).
29. Baker, R. T. K., Lund, C. R. F., and Chludzinski, J. J., *J. Catal.* **87,** 255 (1984).
30. Chu, X., and Schmidt, L. D., to be published.
31. Krause, K., and Schmidt, L. D., *Catal. Lett.*, in press.
32. Baker, R. T. K., and Sherwood, R. D., and Derouane, *J. Catal.* **75,** 382 (1982).
33. Baker, R. T. K., and Sherwood, R. D., *J. Catal.* **61,** 378 (1980).